Advanced Robotics, Vol. 18, No. 4, pp. 357–381 (2004)

Also available online - www.vsppub.com

Full paper

Energy-preserving control of a passive one-legged running robot

SANG-HO HYON * and TAKASHI EMURA

Department of Bioengineering and Robotics, Graduate School of Engineering, Tohoku University, Aramaki-Aza-Aoba 01, Sendai 980-8579, Japan

Received 24 June 2003; revised 3 October 2003; accepted 2 December 2003

Abstract—Fast and energy-efficient control is an increasingly important and attractive area of research in legged locomotion. In this paper, we present a new simple controller for a planar one-legged passive running robot having a springy leg and a compliant hip joint. The most distinctive advantage of the controller over previously proposed ones is it does not require any pre-planned trajectories nor target dynamics. Instead, it utilizes exact non-linear dynamics. Our results are summarized as follows. First, we propose an energy-preserving control strategy for energy-efficient and autonomous gait generation. This strategy is successfully implemented as a new touchdown controller at the flight phase. Simulation results show that the robot can hop from a wide set of initial conditions. Moreover, the running gaits generated are found to be quasi-periodic orbits, which can be seen in Hamiltonian systems. Since the controlled running gaits exist for every admissible energy level, they have some robustness against disturbances. Next, it is shown that an adaptive control of the touchdown angle, which is similar to a delayed feedback controller for a chaotic system, can asymptotically stabilize these quasi-periodic gaits to the periodic ones of the desired period, with some limitations. In particular, for one-periodic gait, by using some additional adaptive controllers, the robot eventually hops without any control inputs. Since our energy-preserving strategy is clear and implementation of the controller is straightforward, we believe it can be easily applied to a wide class of legged mechanisms.

Keywords: Legged locomotion; passive running; orbital stability; energy-preserving control; quasi-periodic orbit.

1. INTRODUCTION

After Matsuoka and Raibert's works [1, 2], one-legged running robots filled with a leg spring have been widely studied both experimentally [3–5] and theoretically [6–8]. These studies contributed to biomechanics in investigating mechanisms of animal locomotion. On the other hand, it was found that in addition to

*To whom correspondence should be addressed. E-mail: sangho@ieee.org

the leg spring, a hip spring also plays an important role in animal running because it enables the leg to be swung passively [9]. Tompson and Raibert showed that the spring-driven one-legged running robot depicted in Fig. 1 can hop without any inputs, provided the initial conditions are appropriately chosen [10]. Therefore, this is a good template model for the purpose of studying energy-efficient running. However, a numerically determined solution was shown to be marginally stable and eventually fails without controls. Therefore, some suitable controller should be applied to ensure orbital stability.

The first successfull controller was found by Ahmadi and Buehler. They applied Raibert's celebrated Foot Placement Algorithm [2] to this passive running robot model. They realized energy-efficient running in simulation [11] and even performed experiments [12]. However, this controller needs a neutral point, which should be approximated or pre-planned just as described in [2]. On the other hand, François and Samson derived a new controller different from Raibert's [13]. They applied a general control method used in a non-linear oscillatory system, i.e. first constructing a Poincaré map (discrete system), then linearizing it around fixed points and finally applying a linear feedback controller to get asymptotically stable periodic orbits. While François and Samson used approximated linear flow, McGeer used numerically determined passive biped running gaits and extensively studied their stability [14]. However, since the model cannot be integrable, the above examples need approximated models, or approximated periodic solutions, to derive the controllers. Therefore, there remain various output errors arising from modeling errors, and, hence, complete passive running gaits have not been obtained through these controllers.

Motivated by these studies and to overcome the above problems, we present a new simple controller to realize energy-efficient one-legged running [15]. Instead of depending on some pre-calculated periodic solutions, or target (desired) dynamics, here we utilize the dynamics of the original non-linear hybrid system to generate (unknown) natural running gaits.

For this purpose, we propose an energy-preserving control strategy. This means the controller preserves the system energy as much as possible. The most important reason why we use this strategy is that if the system energy is preserved, it is expected that the system autonomously generates natural periodic gaits, just as some

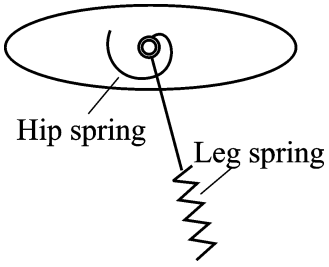

Figure 1. Passive one-legged hopper.

class of Hamiltonian system exhibit natural periodic orbit, even though our system is a complex hybrid dynamical system.

In developing controllers, we chose a simple, but realistic model of a one-legged hopper, the same as that of Ref. [13], which is reviewed in Section 2. In Section 3, we explore the conditions of energy dissipation and normal phase switching for this model, along with our energy preserving control strategy. Then, a new control law to ensure the above conditions, named the non-dissipative touchdown controller, is derived in Section 4. Simulation results and a discussion are also given. In addition, a new controller for asymptotic orbital stabilization to a desired period is proposed and two kinds of adaptation laws for input minimization are presented in Section 5. Section 6 gives a conclusion of the paper.

2. MATHEMATICAL MODEL OF A PASSIVE RUNNING ROBOT

We consider exactly the same model of passive running robot as in Ref. [13] in this paper. In this section, the mathematical model is reviewed.

2.1. Model definition and notation

Figure 2 shows the model of a planar one-legged running robot considered here. The robot is fitted not only with a leg spring, but also a hip spring.

We impose the following assumptions on this model as seen in much of the related literature.

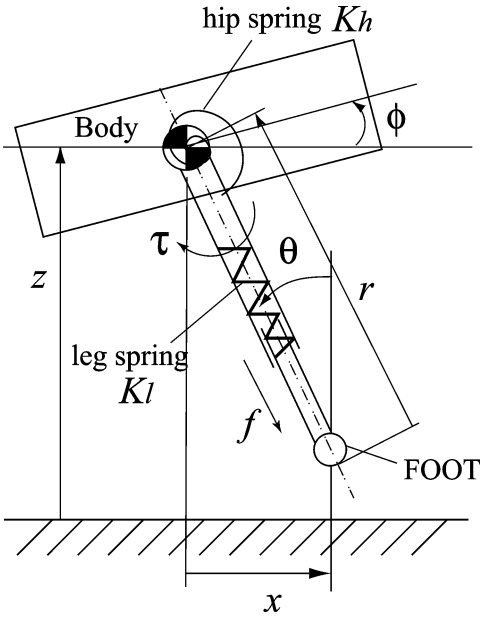

Figure 2. Model definition.

(i) The center of mass (CM) of the body is just on the hip joint and the CM of the leg lies on the leg.

(ii) The mass of the foot (unsprung mass) is negligible.

(iii) The foot does not bounce back nor slip on the ground (inelastic impulsive impact).

(iv) The springs are mass-less and non-dissipating.

We will explain assumptions (ii)–(iv).

Assumption (ii) means the foot of the robot is mass-less and, hence, there is no inertial force due to the foot mass. Of course, this assumption cannot be satisfied exactly in a real machine, but it is rather easy to make the foot lightweight because the the foot is a simple rod.

Thanks to this assumption, there is no impulse along the leg axis. Suppose that the robot performs vertical hopping and the foot touchdowns the ground along the direction of the leg axis. Since the foot is mass-less, it sticks to the ground at the moment of touchdown. In this case, there is no impulse nor kinetic energy loss. Moreover, the robot has a leg spring, which produces a repulsive force once the leg is compressed. Therefore, even when the robot has a small mass on the foot, the spring pushes the foot to the ground. In this case, there may be some small oscillation known as 'chattering'. However, since the chattering can be rapidly recovered by using low restitution material, we can assume the foot sticks to the ground at the moment of touchdown. This is in accordance with observations of our preliminary experiment with our prototype robot, whose foot was made of thin tube fitted with hyper-low restitution rubber.

On the other hand, when the robot receives impact in the perpendicular direction to the longitudinal axis of the leg, energy loss occurs due to the inertia of the 'upper part' of the leg. If the foot is too repulsive, it may bounce back due to this impulse and the robot cannot touchdown the ground appropriately. However, for our robot, it is easy to make the foot lightweight, its restitution low. More importantly, our controller minimizes the touchdown impulse normal to the longitudinal axis of the leg, as shown later. Therefore, assumption (iii) on the inelastic impulse model represents the touchdown dynamics of our one-legged robot most effectively.

Concerning slipping, we assumed large enough friction to simplify the derivation of the controller. It depends on the ground reaction force whether the foot slips the ground or not. If the vector of the reaction force lies within the friction cone, the foot does not slip. However, it is very difficult to predict the reaction force in general, because the dynamics is not integrable. Nevertheless, the development of the controller to avoid slipping under a low-friction environment is not only important, but also challenging work for legged robots and we will explore this problem in the future. Assumption (iv) is not a restrictive one because it is easy to compensate for energy loss by applying leg force f.

Table 1 summarizes the variables that appear in this paper. The equations of motion are composed of four phases: stance phase, lift-off phase, flight phase and

Table 1.
Variables

	Meaning	Unit
x	horizontal position of hip	m
z	vertical position of hip	m
r	leg length	m
ϕ	body angle	rad
θ	leg angle	rad
f	applied force of leg	N
τ	applied torque of hip	N
μ	energy dissipation coefficient	m/s
E	total mechanical energy	J
T_{s}	stance time	s
T_{v}	flight time	s

Table 2.
Subscripts indicating phases

Subscript	Meaning
td−	just before touchdown
td+	just after touchdown
td	just before, or after touchdown
lo	lift-off

Table 3.
Physical parameters

	Meaning	Unit	Value
g	gravity acceleration	$\mathrm{m/s^2}$	9.8
M	total mass	kg	12
r_0	natural leg length	m	0.5
J_{b}	body inertia	$\mathrm{kgm^2}$	0.5
J_{l}	equivalent leg inertia	$\mathrm{kgm^2}$	0.11
K_{l}	leg spring stiffness	N/m	3000
K_{h}	hip spring stiffness	N m/rad	10

touchdown phase. Table 2 defines the phase-indicating subscripts for variables. For example, $\dot{x}_{\mathrm{lo}}$ is the forward velocity of the CM at lift-off, $\dot{\theta}_{\mathrm{td}+}$ is the angular velocity of the leg just before touchdown, θ_{td} is the leg angle of just before or just after touchdown, etc. Table 3 shows the physical parameters, together with the values used in later simulations. Note that J_{l} is an 'equivalent leg inertia' composed of the moment of inertia of the leg mass of the leg, and mass of the body. Let us define the mass of the body as M_{b}, and suppose the leg has mass M_{l} and moment of inertia J_{u}. The mass of the leg is located below the hip joint, with the distance d. Then, 'the

equivalent moment of inertia of leg' J_l is calculated as

$$J_\mathrm{l} = J_\mathrm{u} + \frac{M_\mathrm{b} M_\mathrm{l}}{M_\mathrm{b} + M_\mathrm{l}} d^2.$$

Note that if $d = 0$, then J_l coincides with the leg inertia J_u. For simplicity, we assume total mass $M = M_\mathrm{b} + M_\mathrm{l}$ is located on the hip joint without loss of generality.

2.2. Equation of motion

At the stance phase, the leg compresses and extends, and the angular momentum of the robot around the contact point evolutes under gravity. The dynamics is described as:

$$\begin{cases} M\ddot{r} + K_\mathrm{l}(r - r_0) - Mr\dot{\theta}^2 = Mg(1 - \cos\theta) + f \\ J_\mathrm{l}\ddot{\theta} + J_\mathrm{b}\ddot{\phi} + \dfrac{\mathrm{d}}{\mathrm{d}t}(Mr^2\dot{\theta}) = rMg\sin\theta \\ J_\mathrm{b}\ddot{\phi} + K_\mathrm{h}(\theta - \phi) = \tau_\mathrm{s}, \end{cases} \tag{1}$$

where f is the control force of the leg, while τ_s is the control torque of the hip joint, which are applied during stance. The spring is initially loaded with the same value of gravity force (Mg).

At the flight phase, the CM of the robot moves along a ballistic flight path and the angular momentum of the robot around the CM is preserved. Then, the dynamics is given by:

$$\begin{cases} \ddot{x} = 0 \\ \ddot{z} = -g \\ J_\mathrm{l}\ddot{\theta} + J_\mathrm{b}\ddot{\phi} = 0 \\ J_\mathrm{b}\ddot{\phi} + K_\mathrm{h}(\theta - \phi) = \tau_v, \end{cases} \tag{2}$$

where τ_v represents the control torque of the hip joint, which is applied during flight.

By assumption (iii) in Section 2.1, the velocities of the generalized coordinates change instantaneously at the touchdown phase, according to:

$$\begin{cases} \dot{x}_{\mathrm{td}+} = \dot{x}_{td-} - \dfrac{J_\mathrm{l}\cos\theta_\mathrm{td}}{J_\mathrm{l} + Mr_0^2}\mu_{\mathrm{td}-} \\ \dot{z}_{\mathrm{td}+} = \dot{z}_{td-} - \dfrac{J_\mathrm{l}\sin\theta_\mathrm{td}}{J_\mathrm{l} + Mr_0^2}\mu_{\mathrm{td}-} \\ \dot{\theta}_{\mathrm{td}+} = \dot{\theta}_{\mathrm{td}-} - \dfrac{Mr_0}{J_\mathrm{l} + Mr_0^2}\mu_{\mathrm{td}-} \\ \dot{\phi}_{\mathrm{td}+} = \dot{\phi}_{\mathrm{td}-} \\ \dot{r}_{\mathrm{td}+} = \dot{z}_{\mathrm{td}+}\cos\theta_\mathrm{td} - \dot{x}_{\mathrm{td}+}\sin\theta_\mathrm{td}, \end{cases} \tag{3}$$

where

$$\mu_{\mathrm{td}-} := \dot{x}_{\mathrm{td}-}\cos\theta_{\mathrm{td}} + \dot{z}_{\mathrm{td}-}\sin\theta_{\mathrm{td}} + r_0\dot{\theta}_{\mathrm{td}-}. \tag{4}$$

See Appendix A for derivation of these equations.

At lift-off phase, there are no discontinuous changes except for $\dot{r}_{\mathrm{lo}} = 0$ due to assumption (iii).

3. ANALYSIS ON ENERGY DISSIPATION AND PHASE SWITCHING

If the total mechanical energy is completely preserved and normal phase switching of the system is ensured, it is expected that energy-efficient gaits are autonomously generated. Therefore, preserving energy will be our most important control goal for this purpose and we call this idea the energy-preserving control strategy. However, since energy loss is unavoidable in the real world, we should carefully analyze why and how much energy can be lost. As for the model described in the previous section, energy dissipation occurs for two reasons. One is the control input. Whenever if we apply control input to achieve some control goals, there is always energy consumption. The other reason is the impulsive force imposed at the touchdown phase. In our model, the leg spring cannot absorb the impulse normal to the longitudinal axis of the leg, while it can do along the leg axis.

The energy change between just before touchdown and just after touchdown is uniquely determined by kinetic energy changes. This is because the configuration variables remain constant during the impulse phase and, hence, the potential energy does not change.

$$\begin{aligned}
&E_{\mathrm{td}+} - E_{\mathrm{td}-} \\
&\quad = \left[\frac{1}{2}M(\dot{x}^2 + \dot{z}^2) + \frac{1}{2}J_{\mathrm{b}}\dot{\phi}^2 + \frac{1}{2}J_{\mathrm{l}}\dot{\theta}^2\right]_{\mathrm{td}-}^{\mathrm{td}+} \\
&\quad = \left\{\frac{1}{2}M(\dot{x}_{\mathrm{td}+}^2 + \dot{z}_{\mathrm{td}+}^2) - \frac{1}{2}M(\dot{x}_{\mathrm{td}-}^2 + \dot{z}_{\mathrm{td}-}^2)\right\} + \left(\frac{1}{2}J_{\mathrm{b}}\dot{\phi}_{\mathrm{td}+}^2 - \frac{1}{2}J_{\mathrm{b}}\dot{\phi}_{\mathrm{td}-}^2\right) \\
&\qquad + \left(\frac{1}{2}J_{\mathrm{l}}\dot{\theta}_{\mathrm{td}+}^2 - \frac{1}{2}J_{\mathrm{l}}\dot{\theta}_{\mathrm{td}-}^2\right).
\end{aligned}$$

Substituting (3) into this equation yields:

$$E_{\mathrm{td}+} - E_{\mathrm{td}-} = -\frac{MJ_{\mathrm{l}}}{2(J_{\mathrm{l}} + Mr_0^2)}\mu_{\mathrm{td}-}^2. \tag{5}$$

Therefore, we call $\mu_{\mathrm{td}-}$ the energy dissipation coefficient, because if the condition:

$$\mu_{\mathrm{td}-} = 0, \tag{6}$$

holds at touchdown and no control inputs are applied to the robot, then the total mechanical energy of the system is preserved during running. Therefore, we can say that (6) is a necessary condition for 'complete passive running'.

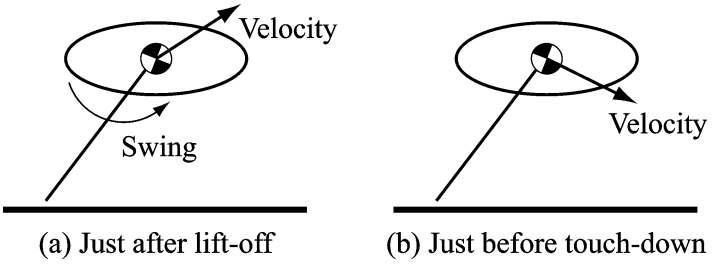

Figure 3. Two kinds of stubbing.

The next important thing we should consider is the condition for sustaining running without falling to the groud. This condition can be defined by the following statements.

(I) Normal phase switching is ensured

(II) Angles of the body and leg at stance phase are bounded within certain region

Condition (I) is very important because our model is a hybrid system, which is mainly composed of two phases — stance phase and flight phase. If the transition between two phases fails, the system cannot evolve anymore. A necessary condition is found to be:

$$\dot{r}_{\mathrm{td}+} < 0. \tag{7}$$

This condition comes from the first equation of (1), which describe the dynamics of the leg length r at the stance phase. In (1), at the moment of touchdown, $Mr\dot{\theta}^2$ and $Mg(1-\cos\theta)$ are positive, and $K_l(r_{\mathrm{td}+}-r_0) = 0$ holds. Therefore, if $\dot{r}_{\mathrm{td}+} > 0$, there are no attractive vector fields that constrain the foot to the ground. This prevents the robot from entering to stance phase from flight phase.

Note that (7) is not always satisfied. Figure 3 shows such two unfortunate situations. Figure 3a indicates stubbing just after lift-off, while Fig. 3b shows stubbing just before touchdown. The situation Fig. 3b cannot be recovered and should be avoided in advance, while the situation in Fig. 3a can be avoided by retracting the leg during the flight phase (since the foot is mass-less, the leg length is arbitrarily controlled 'without influence on the other dynamics').

For the same reason, the axial velocity of the leg just before lift-off must be positive:

$$\dot{r}_{\mathrm{lo}-} > 0. \tag{8}$$

Fortunately, this condition is automatically satisfied if (7) holds because at the stance phase, only repelling force is applied to the direction of the leg axis [16]. Therefore, (7) is sufficient.

Condition (II) is obvious, but it is difficult to derive the sufficient condition mathematically because the dynamics at the stance phase is non-integrable. We will pose this as a future task. Instead, we will limit ourselves to say that this condition could be almost neglected if we suppose no slip occurs between the foot

and ground, as in Section 2.1. Actually, it was never observed in the simulation that condition (II) is violated before the robot lifts off the ground.

4. NON-DISSIPATIVE TOUCHDOWN CONTROL AND QUASI-PERIODIC RUNNING GAITS

4.1. Control goal

If no energy is dissipated during running, the solution curve of this hybrid non-linear system lies on the energy-invariant manifold. If this invariant hybrid flow forms a physically meaningful periodic orbit, it will be the 'gait' we are looking for. For this purpose, we derive a controller to ensure both equations (6) and (7) in this section, and call this new controller 'non-dissipative touchdown control'.

We can do this by applying control inputs only at the flight phase and allowing the robot to move freely at the stance phase with zero inputs. The reason why we are doing so is that if no energy dissipation occurs at touchdown ($\mu_{\mathrm{td}-} = 0$), no interaction between the robot and environment takes place, even if control inputs are applied at the flight phase. Therefore, even if internal energy is not preserved due to the control efforts, the total mechanical energy of the robot 'including the power source of the actuators' is exactly preserved as:

$$\dot{E}_{\mathrm{sys}} := \dot{E} - \tau\dot{\psi} = 0, \tag{9}$$

where τ means control inputs defied by:

$$f = \tau_{\mathrm{s}} = 0, \tag{10}$$

$$\tau_{\mathrm{v}} =: \tau. \tag{11}$$

Our control problem is to find the control input τ that makes the robot land at the time T_{v}, with $(\theta_{\mathrm{td}}, \dot{\theta}_{\mathrm{td}-})$ satisfying (6) and (7), for any given lift-off states $(\dot{x}_{\mathrm{lo}}, \theta_{\mathrm{lo}}, \dot{\theta}_{\mathrm{lo}}, \phi_{\mathrm{lo}}, \dot{\phi}_{\mathrm{lo}})$. Although this is a dead-beat control to bring T_{v}, θ_{td} and $\dot{\theta}_{\mathrm{td}-}$ to the desired values, we only have to choose T_{v} and θ_{td}, because $\dot{\theta}_{\mathrm{td}-}$ is automatically calculated by (6).

There are, however, a large number of such pairs $(T_{\mathrm{v}}, \theta_{\mathrm{td}})$ satisfying (7). Therefore, we determined it by the most simplest way described below. First, we choose T_{v} so that the vertical velocity at touchdown and lift-off is the same in magnitude and opposite in direction:

$$T_{\mathrm{v}} = \frac{2\dot{z}_{\mathrm{lo}}}{g}. \tag{12}$$

Next, we set the desired touchdown angle $\bar{\theta}$ to be symmetric to the lift-off angle about the vertical axis:

$$\bar{\theta} = -\theta_{\mathrm{lo}}. \tag{13}$$

Then, from (6) we obtain the desired touchdown angular velocity $\bar{\dot{\theta}}$ as:

$$\begin{aligned}\dot{\theta}_{\mathrm{td}} &= -\frac{1}{r_0}(\dot{x}_{\mathrm{td}-}\cos\theta_{\mathrm{td}} + \dot{z}_{\mathrm{td}-}\sin\theta_{\mathrm{td}}) \\ &= -\frac{1}{r_0}(\dot{x}_{\mathrm{lo}}\cos\theta_{\mathrm{lo}} + \dot{z}_{\mathrm{lo}}\sin\theta_{\mathrm{lo}}) \\ &= \dot{\theta}_{\mathrm{lo}} =: \bar{\dot{\theta}}. \end{aligned} \tag{14}$$

Additionally, considering:

$$\dot{z}_{\mathrm{td}+} = \dot{z}_{\mathrm{td}-} = \dot{z}_{\mathrm{lo}} - gT_{\mathrm{v}} = -\dot{z}_{\mathrm{lo}}, \tag{15}$$

$$\dot{x}_{\mathrm{td}+} = \dot{x}_{\mathrm{td}-} = \dot{x}_{\mathrm{lo}}, \tag{16}$$

we obtain:

$$\begin{aligned}\dot{r}_{\mathrm{td}+} &= \dot{z}_{\mathrm{td}}\cos\theta_{\mathrm{td}} - \dot{x}_{\mathrm{td}}\sin\theta_{\mathrm{td}} \\ &= -\dot{z}_{\mathrm{lo}}\cos\theta_{\mathrm{lo}} + \dot{x}_{\mathrm{lo}}\sin\theta_{\mathrm{lo}} \\ &= -\dot{r}_{\mathrm{lo}}. \end{aligned} \tag{17}$$

From this, we can see (7) is satisfied as long as we use (12) and (13), and initial conditions are appropriately chosen (described later).

Before closing this section, note again that (12) and (13) are no more than one option. Moreover, this choice does not always results in one-periodic gait. Actually, the variable set that falls into a one-periodic gait (or neutral orbit [8]) is unique for a given energy level and physical parameters.

4.2. Derivation of the controller

Using new variables:

$$\psi = \theta - \phi, \tag{18}$$

$$\sigma = J_{\mathrm{b}}\phi + J_{\mathrm{l}}\theta, \tag{19}$$

the dynamics of flight phase can be rewritten as:

$$\begin{cases} \ddot{x} = 0 \\ \ddot{z} = -g \\ \ddot{\psi} + \Omega_{\mathrm{h}}^2\psi = -\dfrac{\Omega_{\mathrm{h}}^2}{K_{\mathrm{h}}}\tau \\ \ddot{\sigma} = 0. \end{cases} \tag{20}$$

The last equation represents the conservation of the angular momentum of the robot.

Since these are independent second-order linear ODEs, we can easily dead-beat ψ and $\dot{\psi}$, by once-switching of the constant inputs. The reasons why we use dead-beat control are (i) it is optimal from the viewpoint of input magnitude and (ii) it makes it easy to minimize control inputs *via* some adaptive laws as shown in Section 5.2.

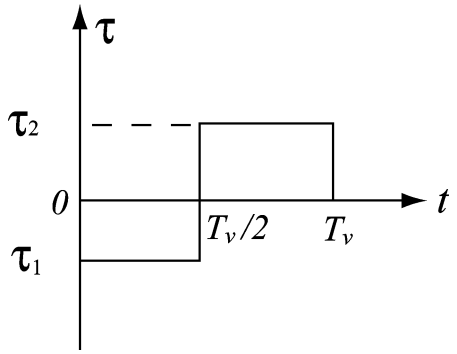

Figure 4. Control input.

Discretizing (20) using piecewise constant inputs (Fig. 4) defied by:

$$\tau = \begin{cases} \tau_1, & \text{if } 0 \leqslant t < T_\mathrm{v}/2 \\ \tau_2, & \text{if } T_\mathrm{v}/2 \leqslant t < T_\mathrm{v}, \end{cases} \tag{21}$$

(where t is the time after the lift-off) and (20), the control inputs can be calculated as:

$$\begin{bmatrix} \tau_1 \\ \tau_2 \end{bmatrix} = B(T_\mathrm{v})^{-1} \left(\begin{bmatrix} \bar{\psi} \\ \dot{\bar{\psi}} \end{bmatrix} - A(T_\mathrm{v}) \begin{bmatrix} \psi_\mathrm{lo} \\ \dot{\psi}_\mathrm{lo} \end{bmatrix} \right), \tag{22}$$

where:

$$\begin{bmatrix} \bar{\psi} \\ \dot{\bar{\psi}} \end{bmatrix} = \frac{1}{J_\mathrm{b}} \left((J_\mathrm{b} + J_\mathrm{l}) \begin{bmatrix} \bar{\theta} \\ \dot{\bar{\theta}} \end{bmatrix} + C(T_\mathrm{v}) \begin{bmatrix} \sigma_\mathrm{lo} \\ \dot{\sigma}_\mathrm{lo} \end{bmatrix} \right), \tag{23}$$

and:

$$A(T_\mathrm{v}) = \begin{bmatrix} \cos(\Omega_\mathrm{h} T_\mathrm{v}) & \dfrac{1}{\Omega_\mathrm{h}} \sin(\Omega_\mathrm{h} T_\mathrm{v}) \\ -\Omega_\mathrm{h} \sin(\Omega_\mathrm{h} T_\mathrm{v}) & \cos(\Omega_\mathrm{h} T_\mathrm{v}) \end{bmatrix}$$

$$B(T_\mathrm{v}) = \frac{1}{K_\mathrm{h}} \begin{bmatrix} \cos(\Omega_\mathrm{h} T_\mathrm{v}) - \cos\left(\dfrac{\Omega_\mathrm{h} T_\mathrm{v}}{2}\right) & -1 + \cos\left(\dfrac{\Omega_h T_\mathrm{v}}{2}\right) \\ \Omega_\mathrm{h} \sin(\Omega_\mathrm{h} T_\mathrm{v}) - \Omega_\mathrm{h} \sin\left(\dfrac{\Omega_\mathrm{h} T_\mathrm{v}}{2}\right) & \Omega_\mathrm{h} \sin\left(\dfrac{\Omega_\mathrm{h} T_\mathrm{v}}{2}\right) \end{bmatrix}$$

$$C(T_\mathrm{v}) = \begin{bmatrix} 1 & T_\mathrm{v} \\ 0 & 1 \end{bmatrix}.$$

Since $\det(B(T_\mathrm{v})) = (\Omega_\mathrm{h}/K_\mathrm{h}^2)\{2\sin(\Omega_\mathrm{h} T_\mathrm{v}/2) - \sin(\Omega_\mathrm{h} T_\mathrm{v})\}$, control inputs (22) always exist, except when $T_\mathrm{v} = 0$ or $T_\mathrm{v} = 2\pi/\Omega_\mathrm{h}$.

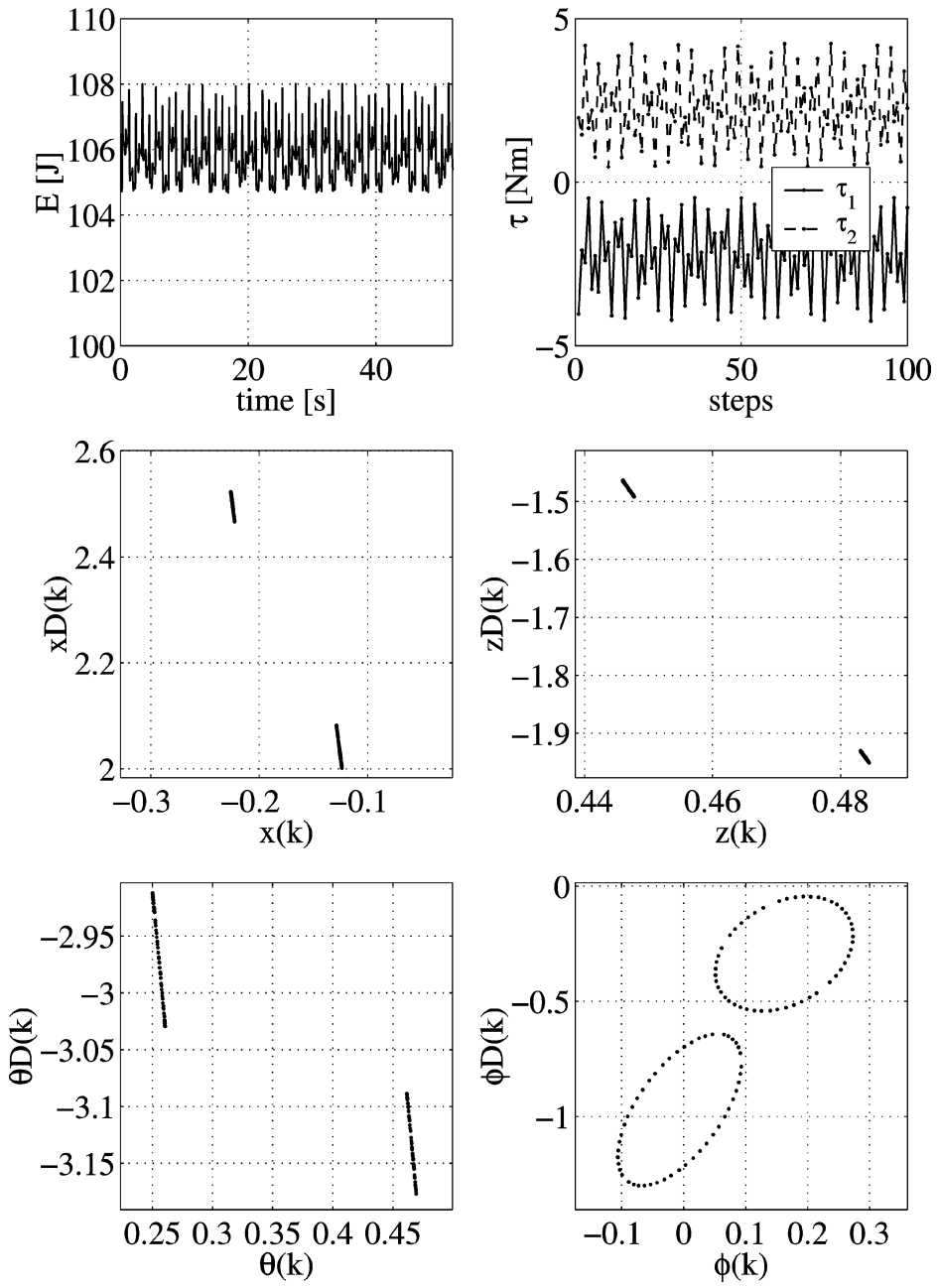

Figure 5. Simulation result of non-dissipative touchdown control. The top two graphs show time evolutions of energy level (E) and control inputs (τ_1 and τ_2). The lower four graphs represent the selected images of the Poincaré map, where notation 'D' represents the time derivatives of preceding variables. Note that the position x is manually reset at each iterative crossing of the section for visibility. Although all the points are bounded in some regions, no fixed points appeared. From this, we can see the gait obtained is a quasi-periodic one.

4.3. Simulation results and discussion

We have simulated the action of the non-dissipative touchdown control (21)–(23), together with (12)–(14), for wide range of initial conditions. The initial condition means the states of just after touchdown hereinafter. Instead of finding them for complete passive running via numerical methods such as Newton–Raphson's method, we just approximate them for the sake of simplicity (see Appendix B).

Figure 5 depicts one of the simulation results. Here, the free parameters of initial values are chosen to be $\theta_0 = 0.25$ rad and $\dot{x}_0 = 2$ m/s. This corresponds to the middle speed of running for the robot of Table 3. We can see from the images of the Ponincaré map that the obtained gaits are quasi-periodic ones, which can be seen in some Hamiltonian systems [17]. Their periods depend on the initial conditions. Since the initial conditions are parameterized in θ_0 and $\dot{x}_0$, we can easily get one-periodic gaits. Figure 6 shows such a pair of parameters. Despite week restrictions to the initial conditions (Appendix B), all solutions starting from them were found to be stable running gaits; thus, the controller allows a wide region of initial conditions. This is also the case for different physical parameter sets. Figure 7 shows stick pictures of high-speed steady running at 5 m/s.

Looking at the time evolution of the energy, the period of the energy level is found to be identical to those of state variables. Since the gaits obtained are non-linear flows on the energy invariant manifold that meets (9):

$$\dot{E}_{\text{sys}} := \dot{E} - \tau\dot{\psi} = 0,$$

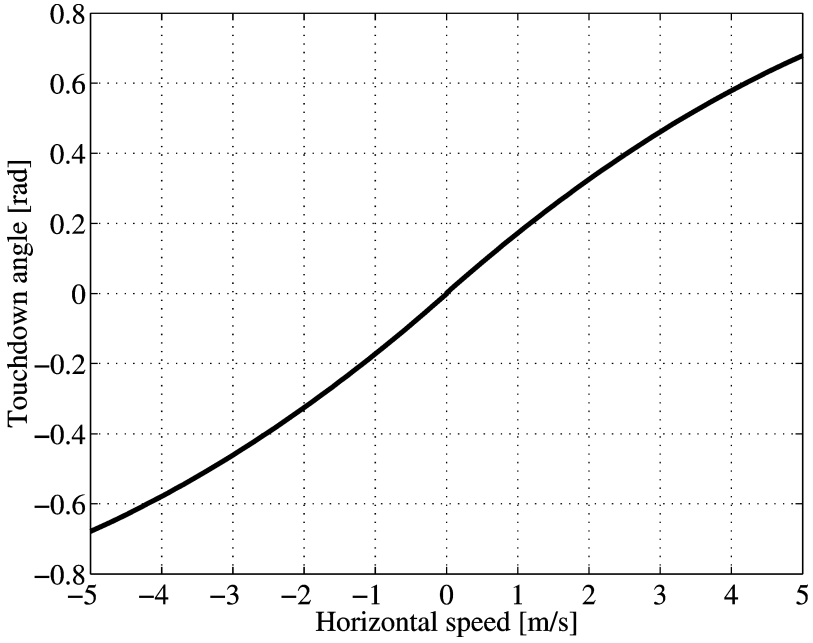

Figure 6. Parameter pairs of complete passive running gaits ($\dot{x}_0$ versus θ_0).

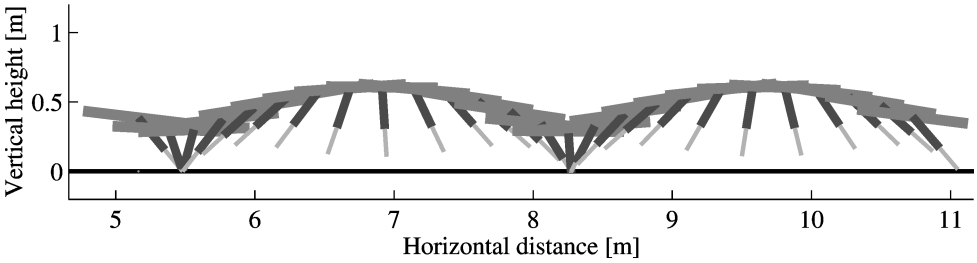

Figure 7. Stick picture of the subsequent two steps of steady running: running speed 5 m/s. The robot moves from left to right.

it is quite natural to ask what happens when there are external disturbances. Figure 8 shows one of the simulation results in the case that we create an external disturbance during running. In this example, a large constant force $f = 200$ N is applied to the robot along to the leg axis at the stance phase (at 30th step). As a result, the energy level is increased by about 25 J. Nevertheless, the robot continues stable running. Note that according to the energy change, the gait has jumped to new quasi-periodic orbits. This robustness against disturbances comes from the fact that our controller does not depend on the energy level itself.

We have also tested a disturbance 'at the flight phase'. However, in many cases, the robot cannot recover the touchdown error and eventually falls down. This be improved when we combine some feedback controllers together with the dead-beat controller.

5. ORBITAL STABILIZATION

Since a one-legged running robot is essentially unstable, stabilization is the most important control goal and we have achieved it in the previous section. However, the obtained gaits are quasi-periodic ones, not limit cycles. Nor are they passive running gaits because the control input has non-zero value. Moreover, they require very large control inputs whenever inappropriate initial conditions are given. In this section, we propose an adaptive orbital stabilization controller and adaptive input minimization controllers.

5.1. Stabilization to a desired periodic orbit by adaptation of the touchdown angle

What should we do to change the period? Remember Section 4.1, where we noted the choice of the desired touchdown angle is not unique. Considering the period of orbits is identical to that of states on the Poincaré section, we invented the following stepwise adaptation law:

$$\overline{\theta(k)} = \begin{cases} -\dfrac{1}{2}(\theta_{\mathrm{lo}}(k) + \theta_{\mathrm{lo}}(k-p)), & \text{if } k > p \\ -\theta_{\mathrm{lo}}(k), & \text{else,} \end{cases} \tag{24}$$

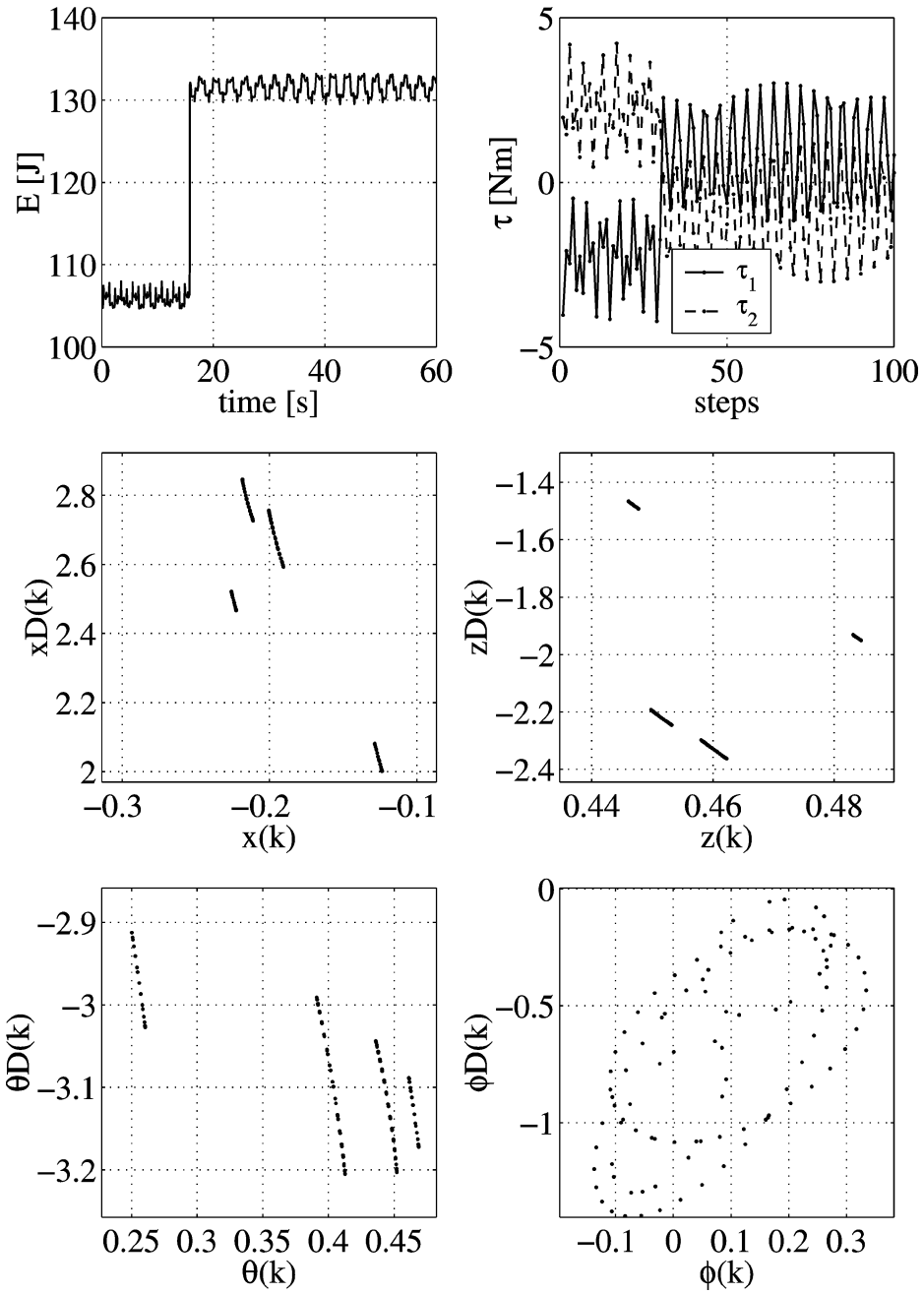

Figure 8. Simulation results of the disturbance test. The top two graphs show time evolutions of energy level (E) and control inputs (τ_1 and τ_2). The lower four graphs represent the selected images of the Poincaré map, where notation 'D' represents the time derivatives of preceding variables. Note that the position x is manually reset at each iterative crossing of the section for visibility. The disturbance is applied at the 30th step, then a new gait appears, which can specified if we compare this with Fig. 5.

where $k \geqslant 1$ is the iteration step and $p \geqslant 1$ is the desired period. The meaning of this adaptation law is clear when considering the case of $p = 1$. In this case, the desired touchdown angle is the negative one half of the summation of the current lift-off angle and the previous lift-off angle. This corresponds to the bisection method in numerical analysis.

We note that this method is incidentally similar to the delayed feedback controller, originally proposed by Pyragas, to stabilize some chaotic orbits to the desired periodic orbit, if we consider the touchdown angle as a control input to the discrete dynamical system (Poincaré map) [18, 19].

5.2. Input minimization via adaptive stiffness control and adaptive leg force control

To minimize control inputs, we focus on the magnitude of the control inputs. Since we are using piecewise control input shown as Fig. 4, input magnitude is represented by a stepwise value:

$$\Delta\tau(k) := \tau_2(k) - \tau_1(k). \tag{25}$$

Considering the robot does not require any control inputs and internal energy is preserved during complete passive running, it can be said that 'if $\Delta\tau$ is increasing, the internal energy is insufficient and vice versa'. Therefore, if we can control the internal energy level appropriately, $\Delta\tau$ could be controlled to zero! We propose two kinds of method below.

The first one is to control spring stiffness adaptively. For example, the hip stiffness adaptation law is given by:

$$\Omega_{\mathrm{h}}(k+1) = \begin{cases} \Omega_{\mathrm{h}}(k) + \gamma_\Omega \cdot \Delta\tau(k), & \text{if } k > 2 \\ \sqrt{K_{\mathrm{h}}\left(\dfrac{1}{J_{\mathrm{b}}} + \dfrac{1}{J_{\mathrm{l}}}\right)}, & \text{if } k = 1, \end{cases} \tag{26}$$

where $\gamma_\Omega > 0$ is the adaptation gain (note that Ω_{h} can be controlled by stiffness of the hip spring K_{h}). If we remember animals can change their joint stiffness via pairs of antagonistic muscles, joint stiffness adaptation (or natural frequency adaptation) may be a quite natural control. In the same manner, the leg spring adaptation law also can be derived.

The second one is to control the internal energy by the external force during the stance phase. For example, (piecewise constant) leg force can be used as:

$$f(k) = \gamma_{\mathrm{f}} \cdot \mathrm{sign}(\Delta\tau(k-1)) \cdot \Delta\tau(k-1), \tag{27}$$

where $\gamma_{\mathrm{f}} > 0$ is the adaptation gain. In the same manner, the hip torque also can be used to produce external force during the stance phase.

Note that the second method changes the total mechanical energy, while the first method does not; it only transfers energy between the controller (motor) and the oscillator of hip spring.

5.3. Simulation results and discussion

First, we will show the stabilization of a two-periodic orbit using (24), under the initial conditions identical to those of Section 4.3. Figure 9 shows the simulation results that actually asymptotically orbitally stabilized to a two-periodic orbit. Interestingly, the energy level is bounded by the range of the original quasi-periodic one.

Next, we will show the result of the stabilization to one-periodic with two kinds of input minimization. Figure 10 shows the simulation, where input minimization via spring stiffness adaptation law (26) is activated from the 60th step. The adaptaion gain γ_Ω was set to 0.1; Figure 11 shows the same plots of input minimization via the leg force adaptation law (27). The adaptaion gain γ_f was set to 40.

We can see from Figs 10 and 11 that both the adaptation laws work well and control inputs eventually converges to zero! Thus, we have succeeded in complete passive running. If we look at the energy level, it converges to 105.3 J in Fig. 10, while in Fig. 11 it jumps from 105.3 J to 111.3 J.

We also tested stabilization to arbitrary periodic gaits and confirmed that for some desired periods, especially for 'the periods of odd number', numerical solutions did not converge. This interesting results will have a relationship with the issue of 'limitation of delayed feedback control' discussed in the literature [19]. Complete passive running was not found for multi-periodic gaits. It was also shown that there are significant differences in convergence speed, depending on the initial conditions or target period. Although we have not yet performed mathematical analysis, we expect the reason lies in the structure of the model. Related to this problem, we refer the reader to Poulakakis *et al*., interesting result [20], where they shows a simplified planar quadruped model has two kind of passive bounding gaits.

6. CONCLUSIONS

We presented a new simple controller for a planar one-legged passive running robot having a telescopic leg and springs.

First, we proposed an energy-preserving control strategy for energy-efficient and autonomous gait generation. This strategy is implemented as a new touchdown controller at the flight phase. Specifically, based on the energy dissipation analysis, non-dissipative touchdown control to ensure energy preservation and normal phase switching was derived. Simulation results shows that the robot can hop from a wide set of initial conditions and the generated running gaits are found to be quasi-periodic orbits, which can be seen in Hamiltonian systems. Since controlled running gaits exist for every admissible energy level, they have some robustness against disturbances.

Next, it was shown that simple adaptation laws, similar to delayed feedback controllers for chaotic systems, can asymptotically stabilize these quasi-periodic gaits to the periodic ones of a desired period, with some limitations. In particular, espe-

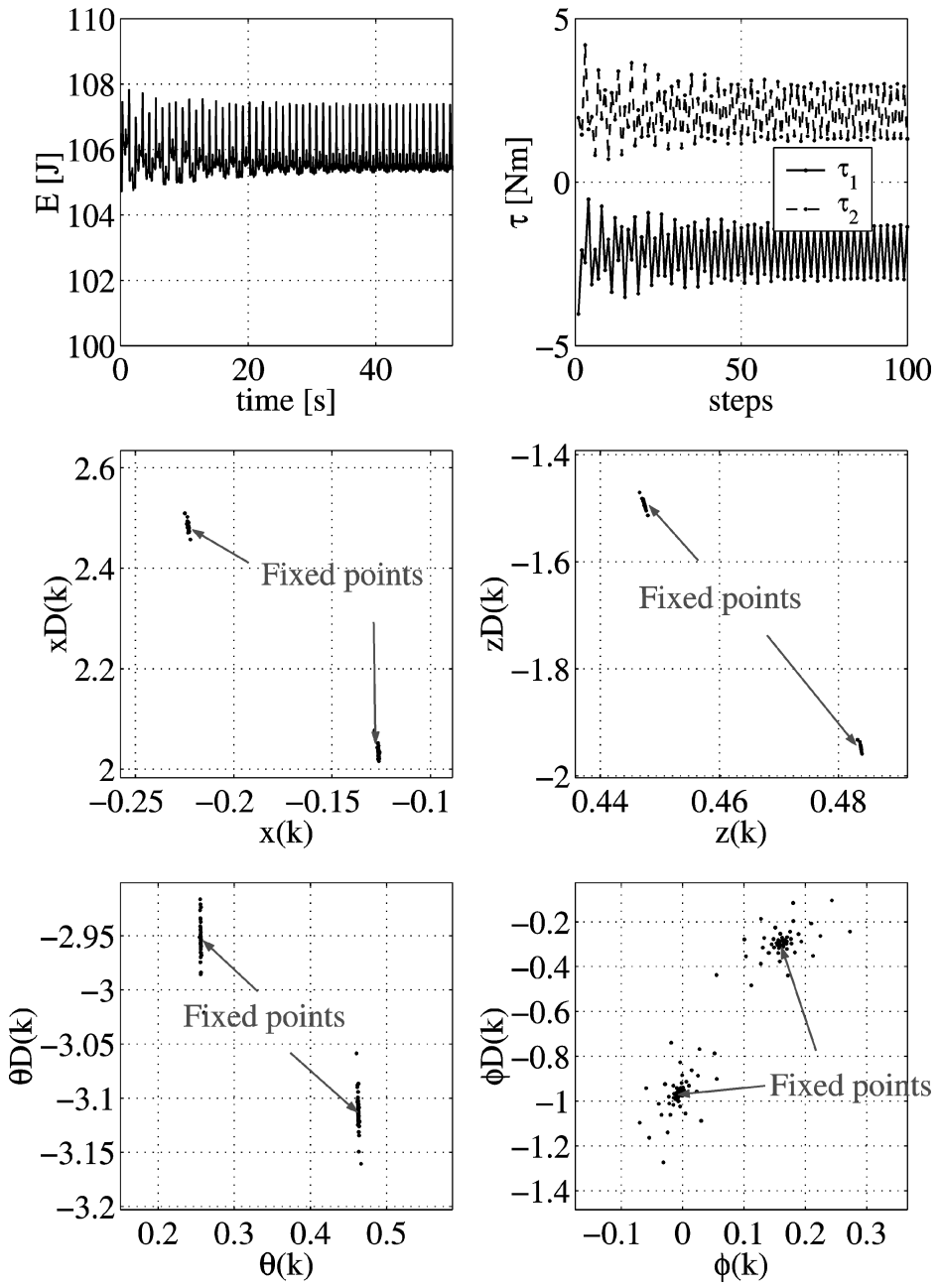

Figure 9. Simulation results of the orbital stabilization to a two-periodic gait. The top two graphs show time evolutions of energy level (E) and control inputs (τ_1 and τ_2). The lower four graphs represent the selected images of the Poincaré map, where notation 'D' represents the time derivatives of preceding variables. Note that the position x is manually reset at each iterative crossing of the section for visibility. The images of the Poincaré map asymptotically converge to two fixed points. This means we have a stable two-periodic orbit.

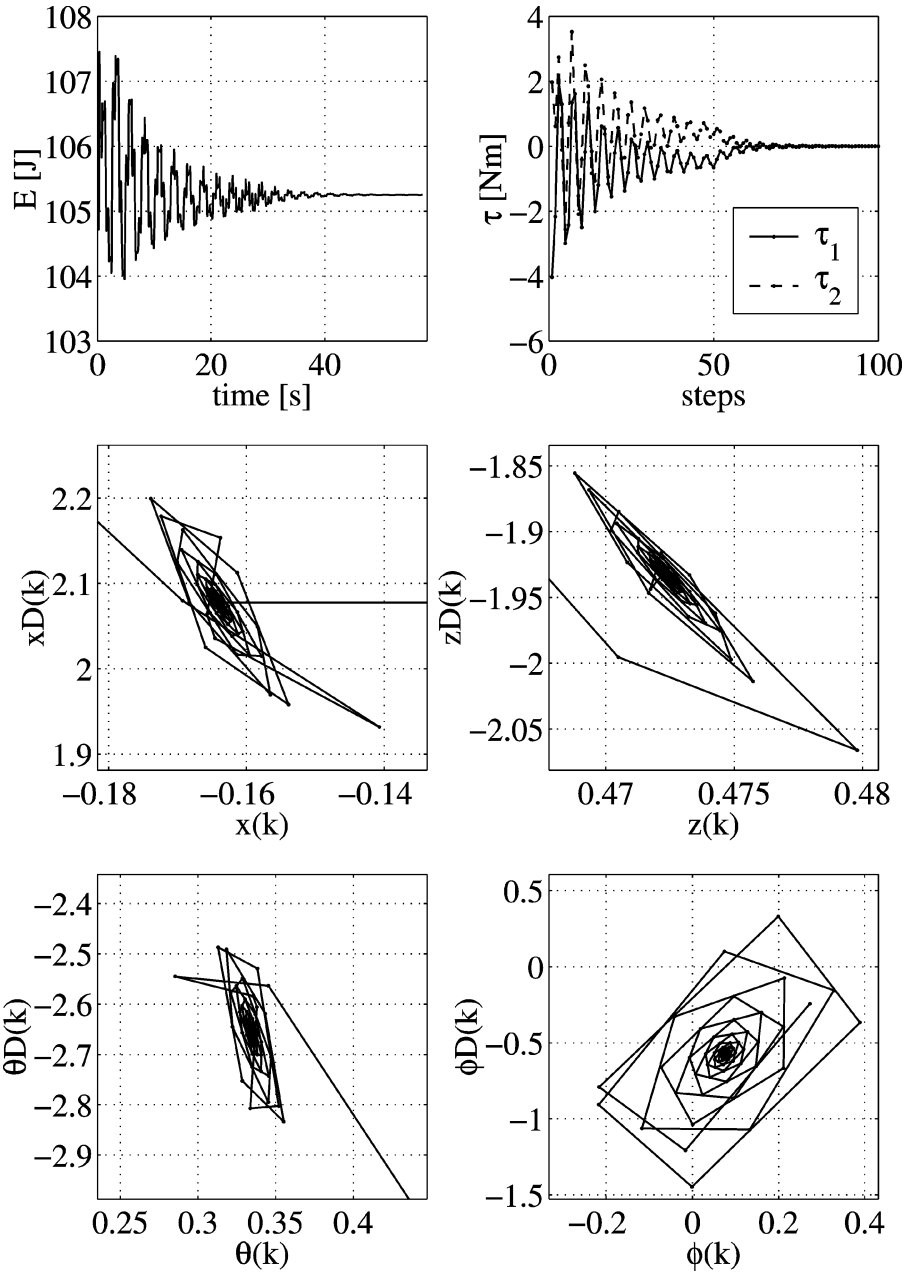

Figure 10. Simulation results of the orbital stabilization controller and the spring stiffness adaptation. The top two graphs show time evolutions of energy level (E) and control inputs (τ_1 and τ_2). The lower four graphs represent the selected images of the Poincaré map, where notation 'D' represents the time derivatives of preceding variables. Note that the position x is manually reset at each iterative crossing of the section for visibility. The input minimization via the spring stiffness adaptation law (26) is activated from the 60th step. The images of Poincaré map asymptotically converge to one fixed point and the control inputs eventually converge to zero!

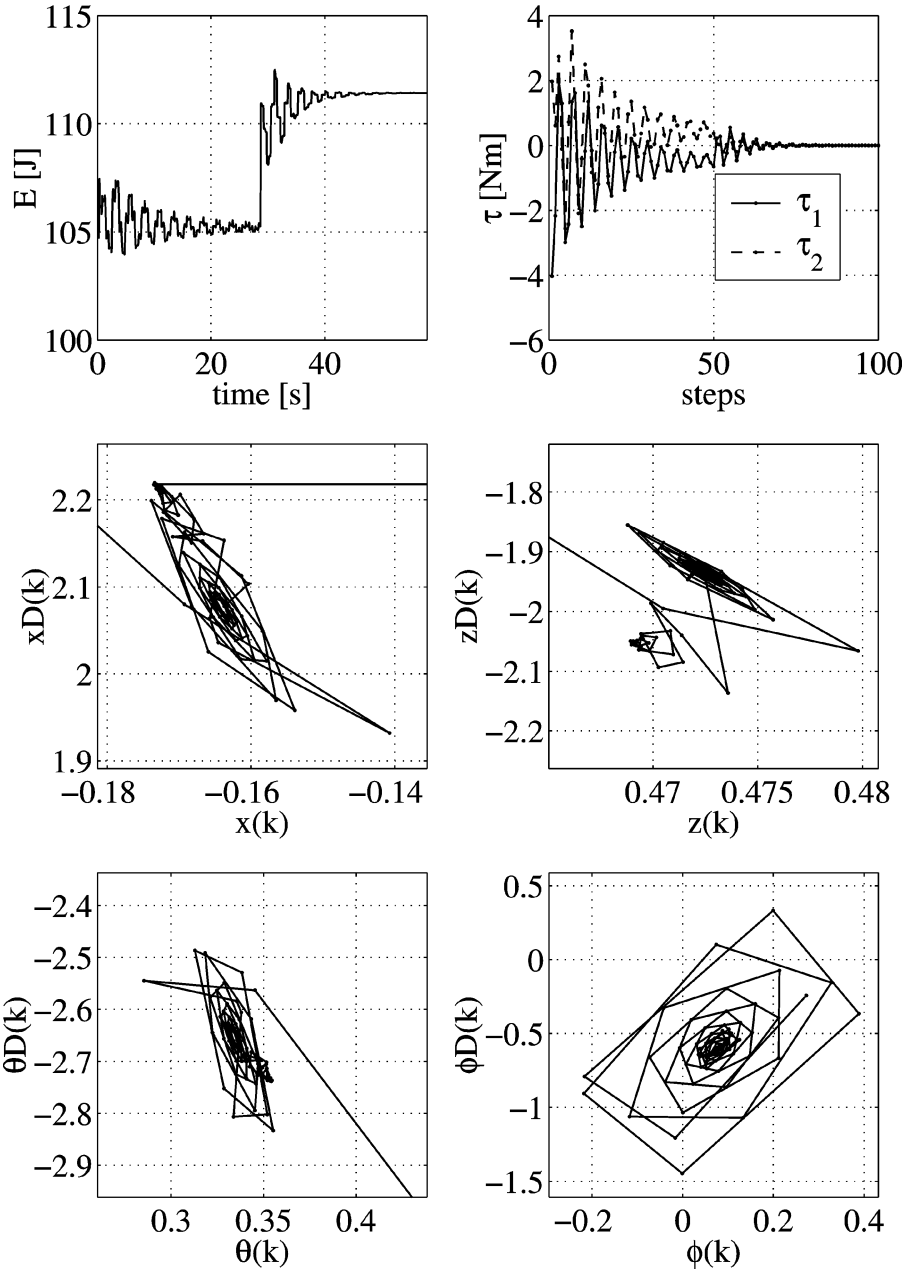

Figure 11. Simulation results of the orbital stabilization controller and the leg force adaptation. The top two graphs show time evolutions of energy level (E) and control inputs (τ_1 and τ_2). The lower four graphs represent the selected images of the Poincaré map, where notation 'D' represents the time derivatives of preceding variables. Note that the position x is manually reset at each iterative crossing of the section for visibility. The input minimization via the leg force adaptation law (27) is activated from the 60th step. Different from Fig. 10, the fixed point is slightly shifted to another point due to the energy change. Nevertheless, control inputs eventually converge to zero!

cially for the one-periodic gait, by applying adaptation laws, the robot eventually hops without any control inputs.

Since our energy-preserving strategy is clear and implementation of the controller is straightforward, we believe it can be easily applied to a wide class of legged mechanisms [21]. We are now constructing experimental models of one-legged and biped robots to verify the controller [22].

Acknowledgement

S.-H. H. thanks to Claude Samson for discussion about literature [13].

REFERENCES

1. K. Masuoka, A mechanical model of repetitive hopping movements, *Biomechanics* **5**, 251–258 (1980) (in Japanese).
2. M. Raibert, *Legged robots that balance*. MIT Press, Cambridge, MA (1985).
3. J. Hodgins and M. Raibert, Biped gymnastics, *Int. J. Robotics Res.* **9** (2), 115–132 (1990).
4. G. Zeglin and B. Brown, Control of a bow leg hopping robot, in: *Proc. Int. Conf. on Robotics and Automation*, Leuven, pp. 793–798 (1998).
5. S. H. Hyon, T. Emura and T. Mita, Dynamics-based control of one legged hopping robot, *J. Syst. Control Engng* **217** (2), 83–98 (2003).
6. D. Koditschek and M. Buehler, Analysis of a simplified hopping robot, *Int. J. Robotics Res.* **10** (6), 587–605 (1991).
7. R. M'Closkey and J. Burdick, Periodic motions of a hopping robot with vertical and forward motion, *Int. J. Robotics Res.* **12** (3), 197–218 (1993).
8. W. Schwind and D. Koditschek, Control of forward velocity for a simplified planar hopping robot, in: *Proc. Int. Conf. on Robotics and Automation*, Nagoya, pp. 691–696 (1995).
9. R. Alexander, Three uses for springs in legged locomotion, *Int. J. Robotics Res.* **9** (2), 53–61 (1990).
10. C. Thompson and M. Raibert, Passive dynamic running, in: *Experimental Robotics I*, V. Hayward and O. Khatib (Eds), pp. 74–83. Springer, Berlin (1989).
11. M. Ahmadi and M. Buehler, Stable control of a simulated one-legged running robot with hip and leg compliance, *Trans. Robotics Automat.* **13** (1), 96–104 (1997).
12. M. Ahmadi and M. Buehler, The ARL Monopod II running robot: control and energetics, in: *Proc. Int. Conf. on Robotics and Automation*, Antwerpen, pp. 1689–1694 (1999).
13. C. François and C. Samson, A new approach to the control of the planar one-legged hopper, *Int. J. Robotics Res.* **17** (11), 1150–1166 (1998).
14. T. McGeer, Passive bipedal running, in: *Proc. Royal Society of London: Biological Sciences* (1990).
15. S. Hyon and T. Emura, Quasi-periodic gaits of passive one-legged hopper, in: *Proc. Int. Conf. on Intelligent Robotics and Systems*, Lausanne, pp. 2625–2630 (2002).
16. H. Goldstein, C. Poole and J. Safko, *Classical Mechanics*, 3rd edn. Addison-Wesley, Reading, MA (2002).
17. V. I. Arnold, *Mathematical Methods of Classical Mechanics*. Springer, Berlin (1978).
18. K. Pyragas, Continuous control of chaos by self-controlling feedback, *Phys. Lett.* **A170**, 421–428 (1992).
19. T. Ushio, Limitation of delayed feedback control in nonlinear discrete-time systems, *Trans. Circ. Sys.* I **43**, 815–816 (1996).

20. I. Poulakakis, E. Papadopoulos and M. Buehler, On the stable passive dynamics of quadruped running, in: *Proc. Int. Conf. on Robotics and Automation*, Taipei, pp. 1368–1373 (2003).
21. S. Hyon and T. Emura, Aerial posture control for 3D biped running using compensator around yaw axis, in: *Proc. Int. Conf. on Robotics and Automation*, Taipei, pp. 57–62 (2003).
22. T. Emura, S. Hyon, Y. Kuroda and M. Suzuki, A biped hopper controlled around yaw axis by body-twisting motion, in: *Proc. Int. Conf. on Mechatronics*, Longhborough, pp. 505–510 (2003).
23. T. McGeer, Passive dynamic walking, *Int. J. Robotics Res.* **9** (2), 62–82 (1990).
24. A. Goswami, B. Espiau and A. Keramame, Limit cycles and their stability in a passive biped gait, in: *Proc. Int. Conf. on Robotics and Automation*, Minneapolis, MN, pp. 246–251 (1996).

APPENDIX A: DERIVATION OF IMPULSE EQUATION (3)

Here, we will derive impulse equation (3). Let us begin with the constrained equation of motion. At the flight phase, equations of motion are described as follows:

$$\begin{cases} M\ddot{x} = 0 \\ M\ddot{z} = -Mg \\ J_{\mathrm{l}}\ddot{\theta} + J_{\mathrm{b}}\ddot{\phi} = 0 \\ J_{\mathrm{b}}\ddot{\phi} + K_{\mathrm{h}}(\theta - \phi) = 0, \end{cases} \tag{A.1}$$

where we removed the control input for simplicity.

At the stance phase, the robot has a constraint as:

$$\begin{cases} x + r\sin\theta = 0 \\ z - r\cos\theta = 0. \end{cases} \tag{A.2}$$

Using this constraint, we can obtain constrained equations of motion at the stance phase:

$$\begin{cases} M\ddot{x} = \lambda_x \\ M\ddot{z} = -Mg + \lambda_z \\ J_{\mathrm{l}}\ddot{\theta} + J_{\mathrm{b}}\ddot{\phi} = \lambda_x r\cos\theta + \lambda_z r\sin\theta \\ J_{\mathrm{b}}\ddot{\phi} + K_{\mathrm{h}}(\theta - \phi) = 0, \end{cases} \tag{A.3}$$

where λ_x and λ_z are Lagrange multipliers, which correspond to the ground reaction forces of the horizontal and vertical direction respectively. The coefficient terms of these multipliers are each component of the Jacobian matrix of (A.2). Combining (A.2) and (A.3), we can obtain the same equations (1) as in Section 2.2.

Now, let us derive the impulse equation. The following calculations are based on Lagrange's impulse equation of motion. At inelastic impact, phase constraint appears suddenly. Due to that, the velocities change instantaneously, while the configuration remains unchanged. In our case, constraint means equation (A.2), i.e. the foot sticks on the ground. This constraint yields an impulsive force (called the constraint impulse). The impulse occurs during a short period of time

$\Delta t := t_{\mathrm{td}+} - t_{\mathrm{td}-}$, i.e. during just before touchdown and just after touchdown. The velocity changes due to the impulse during the time interval Δt can be calculated from (3) to be:

$$\begin{cases} M\Delta\dot{x} = \hat{\lambda}_x \\ M\Delta\dot{z} = \hat{\lambda}_z \\ J_{\mathrm{l}}\Delta\dot{\theta} = \hat{\lambda}_x r\cos\theta + \hat{\lambda}_z r\sin\theta \\ J_{\mathrm{b}}\Delta\dot{\phi} = 0, \end{cases} \tag{A.4}$$

where $\Delta\dot{x} := \dot{x}_{\mathrm{td}+} - \dot{x}_{\mathrm{td}-}$ is the velocity change before/after touchdown. $\Delta\dot{z}$, $\Delta\dot{\theta}$ and $\Delta\dot{\phi}$ are also defined in the same manner. $\hat{\lambda}_x = \int_{t_{\mathrm{td}-}}^{t_{\mathrm{td}+}} \lambda_x \mathrm{d}t$ and $\hat{\lambda}_z = \int_{t_{\mathrm{td}-}}^{t_{\mathrm{td}+}} \lambda_z \mathrm{d}t$ represent the constraint impulse. These equations represent the instantaneous change of kinetic energy due to the impulsive forces.

Remembering impulse is applied only to the perpendicular direction of the longitudinal axis of the leg and there is no impulse to the tangential axis of the leg (see the discussion about our assumption in Section 2.1), we have

$$\begin{cases} \hat{\lambda}_x = \hat{p}\cos\theta \\ \hat{\lambda}_z = \hat{p}\sin\theta, \end{cases} \tag{A.5}$$

where $\hat{p}$ is the impulse normal to the leg axis. Then, (A.4) is re-written as:

$$\begin{cases} M\Delta\dot{x} = \hat{p}\cos\theta \\ M\Delta\dot{z} = \hat{p}\sin\theta \\ J_{\mathrm{l}}\Delta\dot{\theta} = r\hat{p} \\ J_{\mathrm{b}}\Delta\dot{\phi} = 0. \end{cases} \tag{A.6}$$

On the other hand, from the time derivative of (A.2), the following velocity constraint holds just after touchdown.

$$\begin{cases} \dot{x}_{\mathrm{td}+} + \dot{r}_{\mathrm{td}+}\sin\theta_{\mathrm{td}} + r_0\dot{\theta}_{\mathrm{td}+}\cos\theta_{\mathrm{td}} = 0 \\ \dot{z}_{\mathrm{td}+} - \dot{r}_{\mathrm{td}+}\cos\theta_{\mathrm{td}} + r_0\dot{\theta}_{\mathrm{td}+}\sin\theta_{\mathrm{td}} = 0, \end{cases} \tag{A.7}$$

where we used $\theta_{\mathrm{td}} = \theta_{\mathrm{td}-} = \theta_{\mathrm{td}+}$, since the configuration variables do not change during a short period of impact. From this equation, we obtain:

$$\dot{x}_{\mathrm{td}+}\cos\theta_{\mathrm{td}} + \dot{z}_{\mathrm{td}+}\sin\theta_{\mathrm{td}} + r_0\dot{\theta}_{\mathrm{td}+} = 0. \tag{A.8}$$

Substituting (A.6) into (A.8), the constraint impulse normal to the longitudinal axis of the leg is obtained as follows:

$$\left(\dot{x}_{\mathrm{td}+} + \frac{\cos\theta_{\mathrm{td}}}{M}\right)\cos\theta_{\mathrm{td}} + \left(\dot{z}_{\mathrm{td}+} + \frac{\sin\theta_{\mathrm{td}}}{M}\right)\sin\theta_{\mathrm{td}} + r_0\left(\dot{\theta}_{\mathrm{td}+} + \frac{r_0}{J_{\mathrm{l}}}\hat{p}\right) = 0$$

$$\rightarrow \hat{p} = \frac{MJ_{\mathrm{l}}(-\dot{x}_{\mathrm{td}-}\cos\theta_{\mathrm{td}} - \dot{z}_{\mathrm{td}-}\sin\theta_{\mathrm{td}} - r_0\dot{\theta}_{\mathrm{td}-})}{Mr_0^2 + J_{\mathrm{l}}}. \quad \text{(A.9)}$$

From (A.6) and (A.9), we can finally obtain (3).

APPENDIX B: APPROXIMATION OF THE ONE-PERIODIC SOLUTION

The initial conditions for one-periodic passive running could be easily approximated if we suppose synchronization between the two oscillatory motions of leg swinging and compression (see Ref. [11] for details).

Initial conditions to be determined are $(\dot{x}_0, \dot{z}_0, \theta_0, \dot{\theta}_0, \phi_0, \dot{\phi}_0, \dot{r}_0)$, where we choose $(\dot{x}_0, \theta_0)$ as free parameters and let $(\dot{z}_0, \dot{\theta}_0, \phi_0, \dot{\phi}_0, \dot{r}_0)$ be calculated. Supposing that the leg is swung at the natural frequency of the hip spring both at the stance phase and the flight phase yields:

$$\Omega_{\mathrm{h}}(T_s + T_{\mathrm{v}}) = 2\pi, \quad \text{(B.1)}$$

where $\Omega_{\mathrm{h}} := \sqrt{K_{\mathrm{h}}((1/J_{\mathrm{b}}) + (1/J_{\mathrm{l}}))}$ is the natural frequency of leg swinging. Although the stance duration T_{s} depends on the initial conditions at the stance phase, near the vertical running ($\theta \approx 0$), we get:

$$T_{\mathrm{s}} \approx \frac{\pi}{\sqrt{K_{\mathrm{l}}/M}} = \pi/\Omega. \quad \text{(B.2)}$$

Then, flight duration T_{v} becomes:

$$T_{\mathrm{v}} = 2\pi\Omega_{\mathrm{h}} - T_s = \pi\left(\frac{2}{\Omega_{\mathrm{h}}} - \frac{1}{\Omega}\right). \quad \text{(B.3)}$$

From these equations, the initial vertical velocity of the CM is calculated to be:

$$\dot{z}_0 = -2g/T_{\mathrm{v}} = -\frac{2g\pi}{\left(\frac{2}{\Omega_{\mathrm{h}}} - \frac{1}{\Omega}\right)}. \quad \text{(B.4)}$$

Next, from (6), $\dot{\theta}_0$ becomes:

$$\dot{\theta}_0 = -\frac{1}{r_0}(\dot{x}_0\cos\theta_0 + \dot{z}_0\sin\theta_0). \quad \text{(B.5)}$$

Since we assume the natural oscillation of the hip spring, we obtain:

$$\phi_0 = -\frac{J_{\mathrm{l}}}{J_{\mathrm{b}}}\theta_0, \quad \text{(B.6)}$$

$$\dot{\phi}_0 = -\frac{J_1}{Jb}\dot{\theta}_0. \tag{B.7}$$

Finally, from (3), $\dot{r}_0$ is shown to be:

$$\dot{r}_0 = \dot{z}_0 \cos\theta_0 - \dot{x}_0 \sin\theta_0. \tag{B.8}$$

Note that the solutions starting from these approximated initial conditions are not stable except for 'trivial' vertical hopping, i.e. even if we can obtain the exact initial condition for passive running, the robot eventually falls to the ground, because passive running is unstable (the Poincaré map has eigenvalues greater than 1). This is the point that differs most from passive walking robots because they have some basins of attraction, where the robot can walk down a slope without control [23, 24].

ABOUT THE AUTHORS

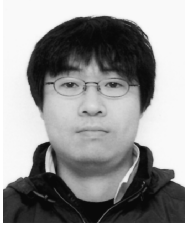

Sang-Ho Hyon received the ME degree from Waseda Univerisity in 1998 and PhD degree from Tokyo Institute of Technology in 2002. He is currently a Research Associate in the Department of Bioengineerign and Robotics of Tohoku University. His research interests include legged locomotion and non-linear dynamical systems. He is a member of the RSJ, JSME, SICE and IEEE.

Takashi Emura received the PhD degree from Tohoku University in 1969. He is currently a Professor in the Department of Bio-Robotics of Tohoku University. He succeeded in walking a biped dynamically and found that the semicircular canal should be defined as an angular velocity sensor from 1972 through 1973. His research interests include legged robots, automatic navigation vehicles, high-precision servomechanism for NC machines, etc. He is a member of the RSJ, JSME, SICE, JSPE and IEEE.